

Influence of Ce Substitution for Bi in BiVO_4 and the Impact on the Phase Evolution and Microwave Dielectric Properties

Di Zhou,^{*,†} Li-Xia Pang,[‡] Jing Guo,[†] Ze-Ming Qi,[§] Tao Shao,[§] Qiu-Ping Wang,^{†,||} Hui-Dong Xie,[⊥] Xi Yao,[†] and Clive A. Randall[#]

[†]Electronic Materials Research Laboratory, Key Laboratory of the Ministry of Education & International Center for Dielectric Research, Xi'an Jiaotong University, Xi'an 710049, Shaanxi, People's Republic of China

[‡]Micro-optoelectronic Systems Laboratories, Xi'an Technological University, Xi'an 710032, Shaanxi, People's Republic of China

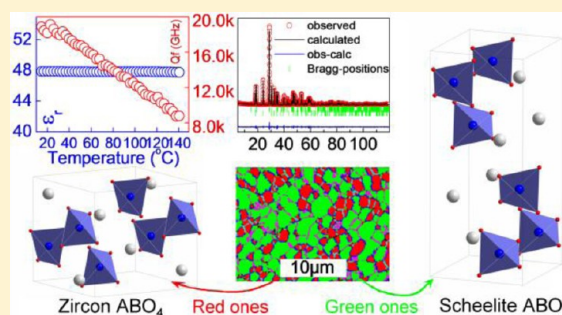
[§]National Synchrotron Radiation Laboratory, University of Science and Technology of China, Hefei 230029, Anhui, People's Republic of China

^{||}School of Science, Xi'an Polytechnic University, Xi'an 710048, Shaanxi, People's Republic of China

[⊥]School of Science, Xi'an University of Architecture & Technology, Xi'an 710055, Shaanxi, People's Republic of China

[#]Center for Dielectric Studies, Materials Research Institute, The Pennsylvania State University, University Park, Pennsylvania 16802, United States

ABSTRACT: In the present work, the $(\text{Bi}_{1-x}\text{Ce}_x)\text{VO}_4$ ($x \leq 0.6$) ceramics were prepared via a solid-state reaction method and all the ceramic samples could be densified below 900 °C. From the X-ray diffraction analysis, it is found that a monoclinic scheelite solid solution can be formed in the range $x \leq 0.10$. In the range $0.20 \leq x \leq 0.60$, a composite region with both monoclinic scheelite and tetragonal zircon solid solutions was formed and the content of the zircon phase increased with the calcined or sintering temperature. The refined lattice parameters of $(\text{Bi}_{0.9}\text{Ce}_{0.1})\text{VO}_4$ are $a = 5.1801(0)$ Å, $b = 5.0992(1)$ Å, $c = 11.6997(8)$ Å, and $\gamma = 90.346(0)^\circ$ with the space group $I1_12/b(15)$. The VO_4 tetrahedron contracts with the substitution of Ce for Bi at the A site, and this helps to keep the specific tetrahedron chain stable in the monoclinic structure. The microwave dielectric permittivity was found to decrease linearly from 68 to about 26.6; meanwhile, the quality factor (Q_f) value increased from 8000 GHz to around 23900 GHz as the x value increased from 0 to 0.60. The best microwave dielectric properties were obtained in a $(\text{Bi}_{0.75}\text{Ce}_{0.25})\text{VO}_4$ ceramic with a permittivity of ~ 47.9 , a Q_f value of ~ 18000 GHz, and a near-zero temperature coefficient of $\sim +15$ ppm/°C at a resonant frequency of around 7.6 GHz at room temperature. Infrared spectral analysis supported that the dielectric contribution for this system at microwave region could be attributed to the absorptions of structural phonon oscillations. This work presents a novel method to modify the temperature coefficient of BiVO_4 -type materials. This system of microwave dielectric ceramic might be an interesting candidate for microwave dielectric resonator and low-temperature cofired ceramic technology applications.



INTRODUCTION

Due to the fast development of mobile communications, satellite communications, radar systems, global positioning systems (GPS), and wireless area network (WLAN) technology, microwave dielectric ceramics have been widely used in dielectric resonators, filters, duplexers, dielectric substrates, etc. To meet the requirements of miniaturization, integration, and high reliability, low-temperature cofired ceramic (LTCC) technology has played a more and more important role in the fabrication of microwave devices. The search for new microwave dielectric ceramics with high performance, low sintering temperature, and low cost has always attracted much attention.^{1–3}

In addition to the novel catalytic properties, the BiVO_4 ceramic was also reported to possess high performance of microwave dielectric properties, with a dielectric relative

permittivity (ϵ_r) of ~ 68 , a quality factor (Q_f) of ~ 6500 – 8000 GHz, a large negative temperature coefficient of resonant frequency (TCF) of -243 to -260 ppm/°C, and a sintering temperature below 900 °C. However, a near-zero temperature coefficient of resonant frequency is necessary for microwave devices used over a wide temperature range. Usually there are two common methods to adjust the TCF values of microwave dielectric ceramics. One is to design composite ceramics with opposite TCF values on the basis of the simple mixing rule. This method works well for the systems with chemical compatibility and similar sintering temperatures, such as the TiO_2 – $\text{Bi}_2\text{Ti}_4\text{O}_{11}$ system,⁴ the ZnNb_2O_6 – TiO_2 system,⁵ the $\text{Ba}_3\text{Nb}_4\text{O}_{15}$ – BaNb_2O_6 system,⁶ etc. The other method is to

Received: October 6, 2013

Published: January 6, 2014

design a solid solution which requires adaptable structures and similar chemical properties and physical properties of ions, such as the $(\text{Bi}_{1-x}\text{Ln}_x)_2\text{Mo}_2\text{O}_9$ ($\text{Ln} = \text{La}, \text{Nd}$) system⁷ and the $[(\text{Li}_{0.5}\text{Bi}_{0.5})_{1-x}\text{Ca}_x]\text{MoO}_4$ system⁸ within the scheelite family, for example. Due to the limited solid solubility, near-zero TCF values can also be achieved by the mixing of solid solutions in many complex systems, such as the $\text{Bi}(\text{Sb}_{1-x}\text{Ta}_x)\text{O}_4$ system⁹ and the $\text{Bi}[\text{Sb}_{1-x}(\text{Nb}_{0.992}\text{V}_{0.008})_x]\text{O}_4$ system,¹⁰ in which both monoclinic BiSbO_4 type and orthorhombic stibiotantalite solid solutions can be formed. In addition to the traditional composite and solid solution methods, a layered ceramic method was frequently also used and demonstrated with ABO_3 ceramics.^{11–13} In our previous work,¹⁴ a permittivity of about 74.8, a high Q_f value of above 11500 GHz, and a TCF value of about +20 ppm/°C were all obtained in the composite $x\text{Bi}(\text{Fe}_{1/3}\text{Mo}_{2/3})\text{O}_4-(1-x)\text{BiVO}_4$ manufactured by mixing the granulated powders (sieved through a mesh screen of 250 μm openings) of $x = 0.02$ and $x = 0.10$ samples, and this method works very well for BVO_4 solid solutions with a composition-dependent ferroelastic phase transition. The BiVO_4 prepared via a solid-state reaction method usually crystallizes in a scheelite monoclinic structure and can reversibly convert to a tetragonal structure at high temperature or high pressure. The BiVO_4 synthesized via wet chemical methods usually forms as a zircon-type tetragonal phase, and it can irreversibly transform to the scheelite monoclinic structure after high-temperature calcinations, which suggests that the zircon-type BiVO_4 is not stable at high temperatures. However, for almost all of the lanthanides, the zircon type LnVO_4 ($\text{Ln} = \text{La}, \text{Ce}, \text{Nd}, \text{Sm}, \text{etc.}$) is quite stable and does not transform to the scheelite monoclinic phase easily. For example, as reported by Panchal et al., the zircon CeVO_4 (which has a larger cationic radius) follows a different sequence of transitions, from zircon to monazite to scheelite, under pressure.¹⁵ As reported by Hirata and Watanabe,¹⁶ a zircon solid solution can be formed in $(\text{Ce}_{1-x}\text{Bi}_x)\text{VO}_4$ within $x \leq 0.60$. However, no details of the X-ray results and phase diagram for the complete $(\text{Ce}_{1-x}\text{Bi}_x)\text{VO}_4$ system have been reported. In the present work, the $(\text{Bi}_{1-x}\text{Ce}_x)\text{VO}_4$ ($x \leq 0.6$) ceramics were prepared via a solid-state reaction method to obtain temperature-stable microwave dielectric ceramics. The sintering behaviors, phase evolutions, and microwave dielectric properties were all studied in detail with associations made with the respective structure and compositional trends.

EXPERIMENTAL SECTION

Proportionate amounts of the reagent-grade starting materials Bi_2O_3 (>99%, Shu-Du Powders Co. Ltd., Chengdu, People's Republic of China) and V_2O_5 and CeO_2 (>99%, Sinopharm Chemical Reagent Co., Ltd., Shanghai, People's Republic of China) were measured according to the stoichiometric formulation $(\text{Bi}_{1-x}\text{Ce}_x)\text{VO}_4$ ($x \leq 0.6$) (abbreviated here as BCV_x). Powders were mixed and milled for 4 h using a planetary mill (Nanjing Machine Factory, Nanjing, People's Republic of China) by setting the running speed at 150 rpm with zirconia balls (2 mm in diameter) as milling media. The powder mixture was then dried and calcined at 650 °C for 4 h. The calcined powders were ball-milled for 5 h with a running speed at 200 rpm to obtain fine powders. Then the powders were then pressed into cylinders (10 mm in diameter and 4–5 mm in height) in a steel die with 5 wt % PVA binder addition under a uniaxial pressure of 20 MPa. Samples were sintered in the temperature range from 740 to 900 °C for 2 h. Room-temperature XRD was performed using an XRD instrument with $\text{Cu K}\alpha$ radiation (Rigaku D/MAX-2400 X-ray diffractometry, Tokyo, Japan). Prior to examination the sintered pellets were crushed in a mortar and pestle to a powder. Diffraction

patterns were obtained between 5 and 65° (2θ) at a step size of 0.02°. To examine the grain morphology, as-fired surfaces were examined by scanning electron microscopy (SEM; JSM-6460, JEOL, Tokyo, Japan). The surface of the BVC0.20 sample was prepared for electron back-scattered diffraction (EBSD), through grinding and polishing with diamond paste and then through lapping for 2 h using a colloidal silica suspension (grain size 10 nm). The Raman spectra at room temperature were obtained on polished pellets with a Raman spectrometer (inVia, Renishaw, England), excited by an Ar^+ laser (514.5 nm). The room-temperature infrared reflectivity spectra were measured using a Bruker IFS 66v FT-IR spectrometer on the infrared beamline station (U4) at the National Synchrotron Radiation Laboratory (NSRL), People's Republic of China. Dielectric properties at microwave frequency were measured with the $\text{TE}_{01\delta}$ dielectric resonator method with a network analyzer (HP 8720 Network Analyzer, Hewlett-Packard) and a temperature chamber (Delta 9023, Delta Design, Poway, CA). The temperature coefficient of resonant frequency TCF (τ_f) was calculated with the formula

$$\text{TCF}(\tau_f) = \frac{f_T - f_{T_0}}{f_{T_0} \times (T - T_0)} \times 10^6 \quad (1)$$

where f_T and f_{T_0} are the $\text{TE}_{01\delta}$ resonant frequencies at temperatures T and T_0 , respectively.

RESULTS AND DISCUSSION

Figure 1 presents the X-ray diffraction patterns of $(\text{Bi}_{1-x}\text{Ce}_x)\text{VO}_4$ ($x = 0.10, 0.20, 0.25, 0.30, 0.40, 0.60$) ceramics calcined at 650 °C and sintered at different temperatures. As reported by Shannon, the ionic radii of Bi^{3+} and Ce^{3+} are 1.17 and 1.143 Å, respectively, in an octahedral coordination environment. As shown in Figure 1, although having the same electrovalence and a little smaller ionic radius, the Ce^{3+} can only partially substitute for the Bi^{3+} ions in the monoclinic BiVO_4 . Even in the sample $(\text{Bi}_{0.9}\text{Ce}_{0.1})\text{VO}_4$, a slight trace of a zircon-type tetragonal phase could be revealed at a 2θ angle of 24.2°, which means that the monoclinic scheelite solid solution of $(\text{Bi}_{1-x}\text{Ce}_x)\text{VO}_4$ can only be formed within $x \leq 0.1$. Different from the results of the $(\text{A}_{0.5x}\text{Bi}_{1-0.5x})(\text{Mo}_x\text{V}_{1-x})\text{O}_4$ ($\text{A} = \text{Li}, \text{Na}, \text{K}$) and $\text{Bi}(\text{Fe}_{x/3}\text{Mo}_{2x/3}\text{V}_{1-x})\text{O}_4$ systems with B site substitution by larger ions reported in our previous work,^{14,17–19} there is no phase transition from the monoclinic to tetragonal scheelite structure observed with the substitution of Ce^{3+} for Bi^{3+} on the A site, and this result confirms that the ferroelastic phase transition from a monoclinic to a tetragonal structure was dominated by the $[\text{BO}_4]$ tetrahedron chains. As the x value increased, the intensity of the zircon-type tetragonal phase increased continuously, while the intensity of the monoclinic scheelite phase decreased. When $x = 0.60$, the main peaks of the monoclinic scheelite phase can hardly be observed, which means the solid solubility of Bi^{3+} in the $(\text{Bi}_{1-x}\text{Ce}_x)\text{VO}_4$ zircon-type tetragonal phase is around 40%; this is much larger than that of Ce^{3+} in the $(\text{Bi}_{1-x}\text{Ce}_x)\text{VO}_4$ monoclinic scheelite phase. The XRD results for the sintered samples are slightly different from that of calcined samples. As shown in Figure 1b, the weak trace of the zircon-type tetragonal phase cannot be observed in $(\text{Bi}_{0.9}\text{Ce}_{0.1})\text{VO}_4$ ceramics, which means that the pure scheelite monoclinic solid solution can be formed. For samples with $x = 0.2, 0.3, 0.6$, it is obvious that the concentration of the zircon-type tetragonal phase is higher than that of the calcined samples, and this result shows that the phase equilibrium in the $(\text{Bi}_{1-x}\text{Ce}_x)\text{VO}_4$ ceramic can be influenced by the temperature. To evaluate the concentrations of different phases in different compositions, the content ratio of the zircon phase was

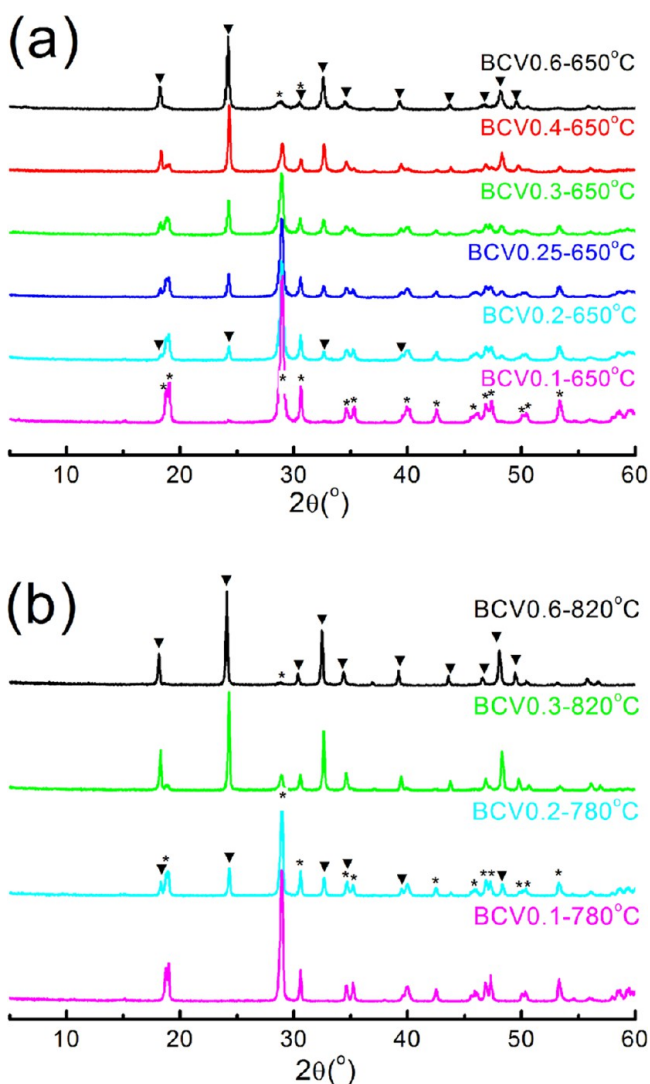


Figure 1. X-ray diffraction data for $(\text{Bi}_{1-x}\text{Ce}_x)\text{VO}_4$ ($x = 0.10, 0.20, 0.25, 0.30, 0.40, 0.60$) ceramics (a) calcined at 650°C and (b) sintered at different temperatures: (*) scheelite monoclinic phase; (▼) zircon-type tetragonal phase.

calculated approximately using the following equation according to the intensity of the highest X-ray peak:

$$\text{content of zircon phase} = I_{z(200)} / (I_{z(200)} + I_{s(112)}) \quad (2)$$

The schematic crystal structures of scheelite and zircon phases and the associated pseudophase diagram are shown in Figure 2. It is obvious that the high temperatures can effectively enhance the zircon content in $(\text{Bi}_{1-x}\text{Ce}_x)\text{VO}_4$ ceramics within $0.1 < x \leq 0.6$. To study the influence of Ce substitution for Bi in BiVO_4 on the crystal structure details, refinements were carried out using Fullprof software on the basis of the fine X-ray diffraction data of BCV0.1 and BCV0.2 samples. The observed and calculated X-ray powder diffraction patterns are shown in Figure 3. The refined values of lattice parameters are $a = 5.1801(0)$ Å, $b = 5.0992(1)$ Å, $c = 11.6997(8)$ Å, and $\gamma = 90.346(0)^\circ$ for the $(\text{Bi}_{0.9}\text{Ce}_{0.1})\text{VO}_4$ sample with the space group $I1_2/b(15)$ using the data (ICSD #100602) reported by Sleight et al. as a starting model.²⁰ The refined lattice parameters for the scheelite and zircon phases $(\text{Bi}_{0.9}\text{Ce}_{0.1})\text{VO}_4$ and $(\text{Ce}_{0.65}\text{Bi}_{0.35})\text{VO}_4$ compositions were supposed) in the $(\text{Bi}_{0.8}\text{Ce}_{0.2})\text{VO}_4$ sample are $a = 5.1741(0)$ Å, $b = 5.1055(0)$

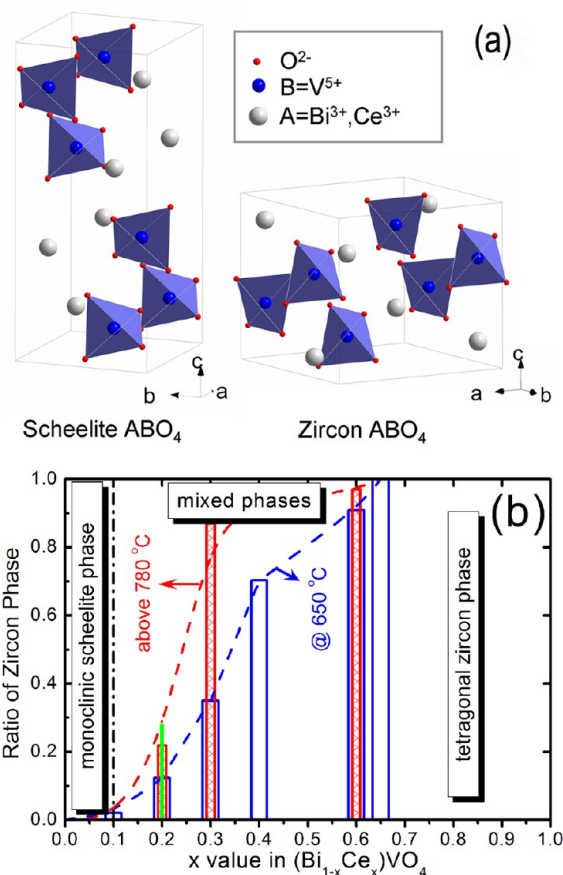


Figure 2. (a) Schematic crystal structures of scheelite and zircon phases and (b) the pseudo phase diagram of the $\text{BiVO}_4\text{-CeVO}_4$ system. The blank bars, reseau bars, and solid line at $x = 0.2$ represent the zircon phase contents in samples calcined at 650°C , sintered at above 780°C , and calculated by Fullprof software, respectively.

Å, $c = 11.7054(4)$ Å, and $\gamma = 90.305(0)^\circ$ with space group $I1_2/b(15)$ and $a = b = 7.3278(4)$ Å and $c = 6.4680(3)$ Å with space group $I4_1/amd(141)$ using the data (ICSD #100733) reported by Dreyer et al.²¹ as the starting model, respectively. All of the atomic fractional coordinates and structure details are given in Tables 1–3. In comparison with the pure BiVO_4 , the cell volume of $(\text{Bi}_{0.9}\text{Ce}_{0.1})\text{VO}_4$ is only slightly smaller ($309.04 \text{ \AA}^3 < 309.20 \text{ \AA}^3$), and this is attributed to the smaller ionic radius of Ce^{3+} (1.143 Å) in comparison to that of Bi^{3+} (1.17 Å) with coordination number 8. In the monoclinic scheelite structure, the BO_4 tetrahedra have two O anions at the top, farther apart than those on the bottom, which are located in one tetrahedron and give one long and one short B–O distance. It is interesting to note that the long V–O and short V–O distances in $(\text{Bi}_{0.9}\text{Ce}_{0.1})\text{VO}_4$ are 1.738 and 1.672 Å, respectively, and both are shorter than those of BiVO_4 (1.767 and 1.692 Å). Meanwhile, the (Bi,Ce)–O distances (2.408 and 2.391 Å) in $(\text{Bi}_{0.9}\text{Ce}_{0.1})\text{VO}_4$ are longer than those of BiVO_4 (2.372 and 2.354 Å). These results show that the VO_4 tetrahedron contracts with the substitution of Ce for Bi at the A site in the scheelite structure, which helps to keep the specific tetrahedron chain stable in the monoclinic structure and further confirm that the VO_4 tetrahedron or the equivalent radius of the B site determines the ferroelastic phase transition monoclinic \rightarrow tetragonal scheelite structure.

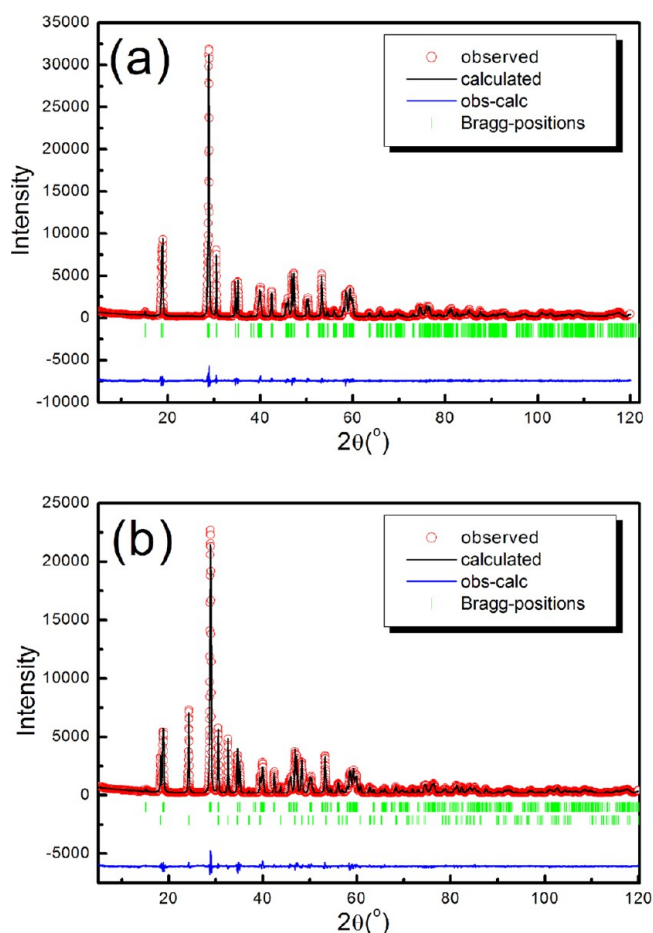


Figure 3. Experimental (circles) and calculated (lines) X-ray powder diffraction profiles for (a) $(\text{Bi}_{0.9}\text{Ce}_{0.1})\text{VO}_4$ and (b) $(\text{Bi}_{0.8}\text{Ce}_{0.2})\text{VO}_4$ compositions at room temperature. $R_p = 7.98$, $R_{wp} = 9.9$, and $R_{exp} = 5.01$ for $(\text{Bi}_{0.9}\text{Ce}_{0.1})\text{VO}_4$, and $R_p = 8.28$, $R_{wp} = 9.98$ and $R_{exp} = 5.56$ for $(\text{Bi}_{0.8}\text{Ce}_{0.2})\text{VO}_4$. The short vertical lines below the patterns mark the positions of Bragg reflections. The bottom continuous line is the difference between the observed and the calculated intensities.

Table 1. Refined Atomic Fractional Coordinates from XRD Data for $(\text{Bi}_{0.9}\text{Ce}_{0.1})\text{VO}_4$ ^a

atom	site	occ	x	y	z
Ce	4e	0.05	0.00000	0.25000	0.63159
Bi	4e	0.45	0.00000	0.25000	0.63159
V	4e	0.50	0.00000	0.25000	0.12882
O1	8f	1.00	0.14698	0.49983	0.20672
O2	8f	1.00	0.25856	0.37879	0.44711

^aThe lattice parameters at room temperature are $a = 5.1801(0)$ Å, $b = 5.0992(1)$ Å, $c = 11.6998(0)$ Å, and $\gamma = 90.346(0)^\circ$. The space group is $I1_12/b(15)$.

SEM micrographs of as-fired surfaces demonstrate the granular microstructure of the $(\text{Bi}_{1-x}\text{Ce}_x)\text{VO}_4$ ceramics ($x = 0.10, 0.10, 0.30$) sintered at different temperatures, as shown in Figure 4. Dense and homogeneous microstructures with almost no porosity could be found in all compositions. The densification temperature increased from 800 °C for BCV0.10 to around 860 °C for BCV0.30 ceramics. The grain size lies between 1 and 5 μm . Due to their similar chemical compositions, the monoclinic scheelite and zircon-type tetragonal phases cannot be readily distinguished from each

Table 2. Refined Atomic Fractional Coordinates from XRD Data for $(\text{Bi}_{0.9}\text{Ce}_{0.1})\text{VO}_4$ (in the $(\text{Bi}_{0.8}\text{Ce}_{0.2})\text{VO}_4$ Sample)^a

atom	site	occ	x	y	z
Ce	4e	0.05	0.00000	0.25000	0.63069
Bi	4e	0.45	0.00000	0.25000	0.63069
V	4e	0.50	0.00000	0.25000	0.12869
O1	8f	1.00	0.14433	0.49127	0.20536
O2	8f	1.00	0.25982	0.38235	0.44584

^aThe lattice parameters at room temperature are $a = 5.1741(0)$ Å, $b = 5.1055(0)$ Å, $c = 11.7054(4)$ Å, and $\gamma = 90.305(0)^\circ$. The space group is $I1_12/b(15)$.

Table 3. Refined Atomic Fractional Coordinates from XRD Data for $(\text{Ce}_{0.65}\text{Bi}_{0.35})\text{VO}_4$ (in the $(\text{Bi}_{0.8}\text{Ce}_{0.2})\text{VO}_4$ Sample)^a

atom	site	occ	x	y	z
Ce	4a	0.08125	0.00000	0.75000	0.12500
Bi	4a	0.04375	0.00000	0.75000	0.12500
V	4b	0.12500	0.00000	0.25000	0.37500
O	16h	0.50000	0.00000	0.07063	0.20540

^aThe lattice parameters at room temperature are $a = 7.3278(4)$ Å, $b = 7.3278(4)$ Å, and $c = 6.4680(3)$ Å. The space group is $I4_1/amd(141)$.

other by backscattered electron images. The EBSD technique was employed for orientation and phase analysis. It is based on an automatic analysis of Kikuchi-type diffraction patterns generated by backscattered electrons. The crystallographic orientation can be determined by indexing the corresponding diffraction pattern. Figure 4c presents the phase map, and the inset shows the crystallographic orientation map for the BVC0.20 sample. The total map size is around 2000 μm^2 . From the inset it is seen that all of the grains scattered randomly and this is quite normal in the polycrystalline samples. It is easily seen that there are two different kinds of grains observed from the phase map. The grains colored green belong to the scheelite phase, and the other grains colored red belong to the zircon phase. The amount of the zircon phase calculated from the EBSD result is around 27%, and this result corresponds well with that obtained from the XRD analysis.

The room-temperature Raman spectra $(\text{Bi}_{1-x}\text{Ce}_x)\text{VO}_4$ ($x = 0.10, 0.20, 0.30, 0.60$) ceramics are shown in Figure 5. For the pure BiVO_4 (space group $I2/a$), nine different Raman-active modes are predicted through the group theory:

$$\Gamma = 3A_g + 6B_g \quad (3)$$

In the spectra of BCV0.1, the strongest mode at 824.1 cm^{-1} is assigned to the symmetric V–O stretching mode $\nu_s(\text{V–O})$ and the weak shoulder at about 725.2 cm^{-1} is assigned to the asymmetric V–O stretching mode $\nu_{as}(\text{V–O})$. The symmetric bending mode $\delta_s(\text{VO}_4)$ and the asymmetric bending mode $\delta_{as}(\text{VO}_4)$ are near 365.1 and 330.5 cm^{-1} , respectively. The external modes (rotation/translation) are observed at 211.9 and 127.2 cm^{-1} , respectively. For the zircon phase (space group $I4_1/amd$, $Z = 4$), group theory predicts 12 distinct Raman-active modes:

$$\Gamma = 2A_{1g} + 4B_{1g} + B_{2g} + 5E_g \quad (4)$$

Raman spectra of BCV0.6 agree with those reported.²² In the spectra of BCV0.6, the strongest mode at 851.8 cm^{-1} is the symmetric stretching mode $\nu_s(\text{V–O})$ (A_{1g} symmetry). The other two modes at around 778.1 cm^{-1} (overlapping) are the asymmetric stretching modes $\nu_{as}(\text{V–O})$ of symmetries E_g and

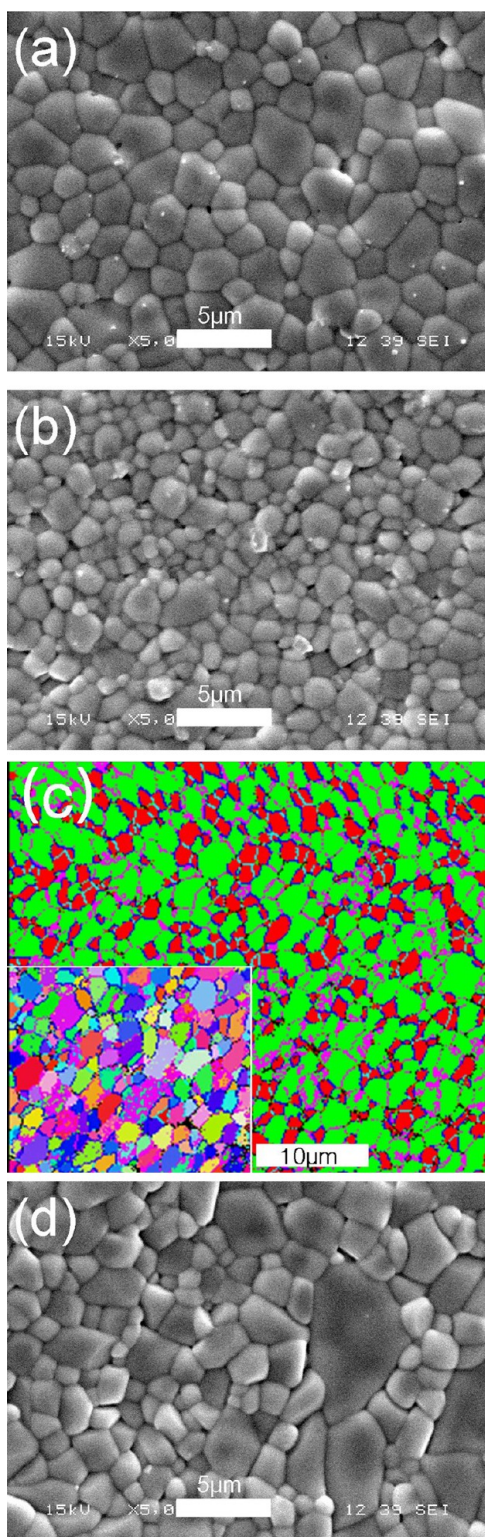


Figure 4. SEM photos of $(\text{Bi}_{1-x}\text{Ce}_x)\text{VO}_4$ ceramics with (a) $x = 0.10$ sintered at $800\text{ }^\circ\text{C}$, (b) $x = 0.20$ sintered at $820\text{ }^\circ\text{C}$ and (c) its phase map plus crystallographic orientation map (insert) obtained from the EBSD analysis, and (d) $x = 0.30$ sintered at $860\text{ }^\circ\text{C}$.

B_{1g} , respectively. The V–O bending modes appear in the range $250\text{--}500\text{ cm}^{-1}$. The mode at 368.5 cm^{-1} is the symmetric bending mode $\delta_s(\text{VO}_4)$ (A_{1g} symmetry), and that at 466 cm^{-1} is the asymmetric bending mode (ν_4) of B_{1g} symmetry; the other asymmetric bending mode of E_g symmetry could not be

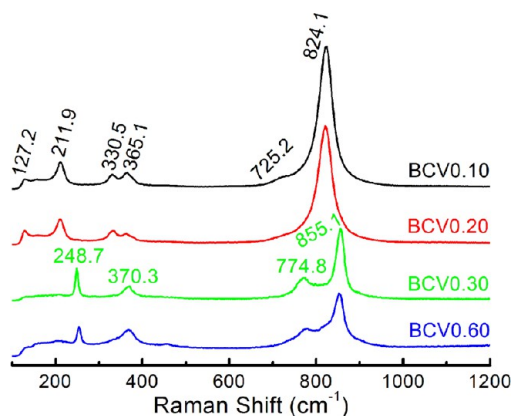


Figure 5. Room-temperature Raman spectra of $(\text{Bi}_{1-x}\text{Ce}_x)\text{VO}_4$ ($x=0.10, 0.20, 0.30, 0.60$) ceramics.

detected. The mode at 253.9 cm^{-1} is the B_{2g} mode due to symmetric bending of the VO_4 tetrahedron. The external modes appear at frequencies below 250 cm^{-1} .^{23–27} Empirical relations²⁸ ($\nu = 21349 \times \exp(-1.9176R)$, where ν is the Raman shift in cm^{-1} and R is the V–O bond length in Å) have been found between the metal–oxygen Raman stretching frequencies and bond lengths for vanadium, and the shorter distance of V–O in zircon phase in comparison to that in the scheelite phase can explain the blue shift of the $\nu_s(\text{V–O})$ mode.

Microwave dielectric relative permittivity and Q_f values of $(\text{Bi}_{1-x}\text{Ce}_x)\text{VO}_4$ ceramics measured at 5–8 GHz are shown in Figure 6 as a function of sintering temperature. As the sintering

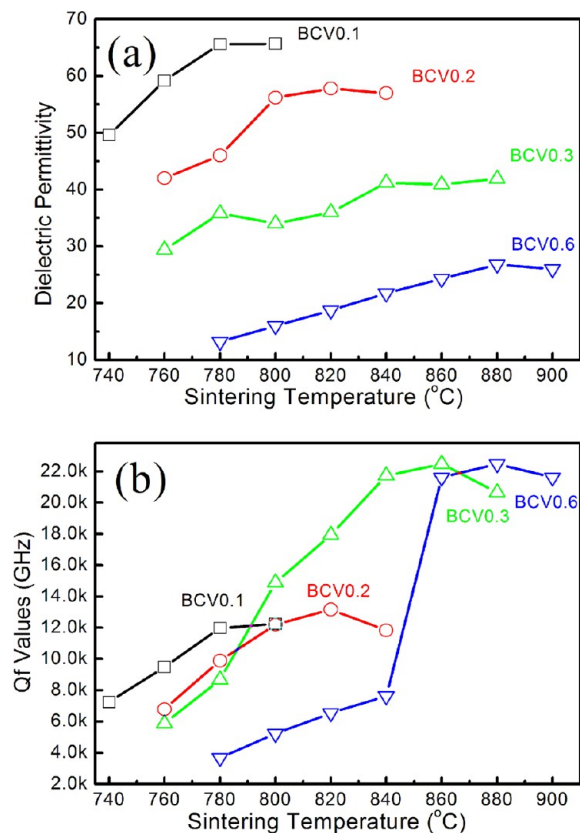


Figure 6. Room-temperature (a) microwave dielectric permittivity and (b) Q_f values of $(\text{Bi}_{1-x}\text{Ce}_x)\text{VO}_4$ ($x = 0.10, 0.20, 0.30, 0.60$) ceramics as a function of sintering temperature.

temperature increases, the microwave dielectric constant increases and then reaches a saturated value, as there is an elimination of the pores. The optimal sintering temperature increases from 780 °C for BCVO.1 to 880 °C for BCVO.6. The sintering temperature of pure CeO₂ is above 1600 °C.²⁹ Hence, it is understandable that the sintering temperatures of (Bi_{1-x}Ce_x)VO₄ ceramics depend on the concentration of Ce as a refractory chemical. The Q_f values are quite sensitive to the sintering temperature because the extrinsic dielectric loss of the ceramic sample is determined by the universal defects caused by the porosity, grain boundary, etc. The optimized sintering process, especially the sintering temperature and incubation or hold times, can help to decrease the extrinsic dielectric loss and enhance the Q_f values. It is seen that the Q_f values of (Bi_{1-x}Ce_x)VO₄ ceramics first increased with the sintering temperature and then reached the maximum values. The microwave dielectric properties of (Bi_{1-x}Ce_x)VO₄ ceramics sintered at optimal temperatures as a function of *x* value are shown in Figure 7. It can be seen that as the *x* value increased

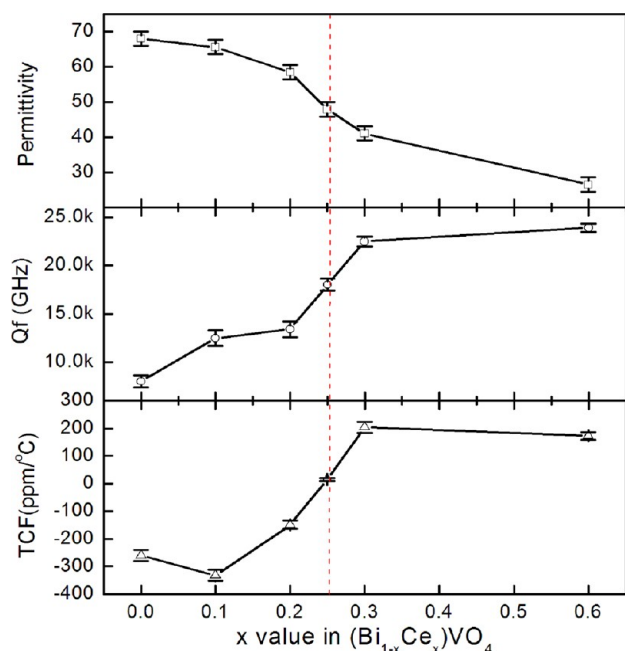


Figure 7. Microwave dielectric permittivity, Q_f, and TCF values of (Bi_{1-x}Ce_x)VO₄ (*x* = 0.10, 0.20, 0.25, 0.30 and 0.60) ceramics as a function of *x*.

from 0.0 to 0.6, the dielectric permittivity decreased from 68 for pure BiVO₄ to about 26.6 for (Bi_{0.4}Ce_{0.6})VO₄ ceramic. The dielectric permittivity is determined by the molecular polarizability, which can be predicted by the ionic polarizability additive rule suggested and developed by Heydweiller and Shannon.^{30,31} As reported by Shannon,³¹ the ionic polarizability of Ce³⁺ is 6.15 Å³, slightly larger than that of Bi³⁺ (6.12 Å³). This is contradictory to the result in the present work. In fact, the polarizability of a certain ion is influenced more strongly by its real structural environment in a compound. The polarizability value of Ce³⁺ reported by Shannon was calculated on the basis of CeF₃, in which the Ce³⁺ ions are coordinated by five F atoms. Its value does not work well for many oxides. According to Shannon's results, the polarizability of ions with a given electrovalence value was found to be proportional to the ion volume. Hence, for the lanthanide, the ionic polarizability in

the same structural environment should decrease with the ionic radius in the order La, Ce, Nd, Sm, etc. However, the ionic polarizability of La³⁺ reported by Shannon is 6.07 Å³, which is also slightly smaller than that of Ce³⁺. In fact, in many solid solution ceramics, in which the Bi³⁺ and lanthanide can occupy the same position, the microwave dielectric permittivity usually decreased with the lanthanide content, such as the (Bi_{1-x}Ln_x)₂Mo₂O₉ (Ln = La, Nd, 0.0 ≤ *x* ≤ 0.2) system, the (Bi,Ln)PO₄ (Ln = La, Ce, Nd, Sm) system, etc. Considering the influence of crystal structure and anisotropy, Feteira et al.³² also provided a series of revised polarizabilities value for lanthanides, among which the largest is 4.69 Å³ for La³⁺, based on the LnAlO₃ (Ln = La, Ce, Pr, Nd, etc.) system. In a word, the polarizability of Bi³⁺ in the microwave region is usually larger than that of lanthanide, especially for the Ce³⁺ here. Hence, it is understandable that the microwave dielectric permittivity of monoclinic scheelite and zircon-type tetragonal solid solutions decreases with the Ce content. As shown in Figure 7, the Q_f values increased from 8000 GHz for pure BiVO₄ to around 23900 GHz for (Bi_{0.4}Ce_{0.6})VO₄ ceramic. According to the classical harmonic oscillator model, the intrinsic dielectric loss caused by absorptions of phonon oscillation within the lattice is proportional to the dielectric permittivity and the optimal Q_f value is dominated by the intrinsic dielectric loss. Hence, it is understandable that the Q_f values of (Bi_{1-x}Ce_x)VO₄ ceramics increase with the permittivity. Although there is no report on the microwave dielectric properties of pure CeVO₄ ceramic, it can be deduced that its Q_f value is much higher than 23900 GHz. As reported in the literature, the Q_f value of a YVO₄ single crystal, which has the same crystal structure as CeVO₄, can reach as high as 280000 GHz at a frequency of 16.3 GHz with a permittivity of ~9.4 and a temperature coefficient of permittivity of around 84 ppm/°C.³³ The TCF value remained around -300 ppm/°C when *x* ≤ 0.10, and this is dominated by the monoclinic scheelite phase. When *x* > 0.1, the zircon tetragonal solid solution started to form and this resulted in the sharp shift of the TCF value to a positive value of around +200 ppm/°C for the (Bi_{0.7}Ce_{0.3})VO₄ ceramic and then remained stable with the disappearance of the scheelite monoclinic phase. The trend of TCF value almost obeys the simple mixing rule.

To better understand the temperature dependence of microwave dielectric properties, the microwave dielectric permittivity, and Q_f value as a function of temperature in the range 20–140 °C are shown in Figure 8. It is seen that the microwave dielectric permittivity of (Bi_{0.75}Ce_{0.25})VO₄ decreased slightly from 47.88 at 20 °C to around 47.74 at 140 °C, which means it is quite stable in wide temperature range and suitable for communication device application. All the Q_f value of (Bi_{1-x}Ce_x)VO₄ ceramics decreased with the temperature, which means the dielectric loss increased with temperature. A little different from the results for *x* ≤ 0.1, the Q_f values for compositions with *x* > 0.1 seems to be more sensitive to the temperature. The best microwave dielectric properties were obtained in (Bi_{0.75}Ce_{0.25})VO₄ ceramic with a permittivity ~47.9, a Q_f value ~18,000 GHz and a near-zero temperature coefficient ~ +15 ppm/°C at a resonant frequency around 7.6 GHz at room temperature.

Figure 9 presents measured and calculated infrared reflectivity spectra of the (Bi_{1-x}Ce_x)VO₄ (*x* = 0.10, 0.20, 0.30, 0.60) ceramics. For all of the spectra, the bands at 600–900 cm⁻¹ can be assigned to ν₁(VO₄) and ν₃(VO₄) and the bands at 200–500 cm⁻¹ can be assigned to ν₂(VO₄) and

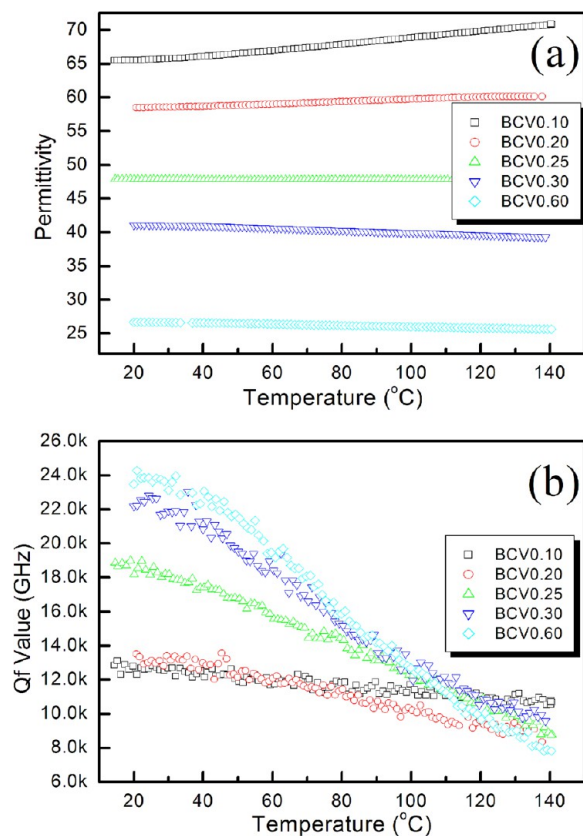


Figure 8. Microwave (a) dielectric permittivity and (b) Q_f values of $(\text{Bi}_{1-x}\text{Ce}_x)\text{VO}_4$ ($x = 0.10, 0.20, 0.25, 0.30, 0.60$) ceramics as a function of temperature in the range 20–140 °C.

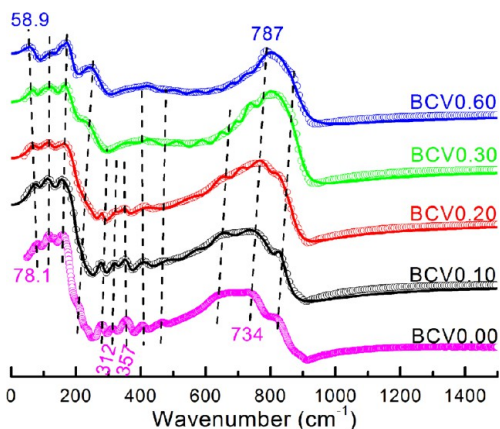


Figure 9. Measured and calculated infrared reflectivity spectra of the $(\text{Bi}_{1-x}\text{Ce}_x)\text{VO}_4$ ($x = 0.10, 0.20, 0.30, 0.60$) ceramics (solid lines for fitted values and circles for measured values).

$\nu_4(\text{VO}_4)$, while the bands below 200 cm^{-1} can be assigned to the Bi–O band.^{24,34–36} The spectra for the BiVO_4 and $(\text{Bi}_{0.4}\text{Ce}_{0.6})\text{VO}_4$ samples are both similar to the reports in the literature. It can be found that with an increase of x value in $(\text{Bi}_{1-x}\text{Ce}_x)\text{VO}_4$ system the $\nu_1(\text{VO}_4)$ and $\nu_3(\text{VO}_4)$ bands move in the high-wavenumber direction, due to the shorter distance of V–O in tetragonal zircon phase in comparison to that in the monoclinic scheelite phase. Of note, the band at 734 cm^{-1} for BiVO_4 blue-shifts to 787 cm^{-1} for $(\text{Bi}_{0.4}\text{Ce}_{0.6})\text{VO}_4$, while the bands at $200\text{--}500\text{ cm}^{-1}$ move to the low-wavenumber direction, due to the longer distance of Ce–O in the tetragonal

zircon phase in comparison to that of Bi–O in the monoclinic scheelite phase; especially the first band at 78.1 cm^{-1} for BiVO_4 red-shifts to 58.9 cm^{-1} for $(\text{Bi}_{0.4}\text{Ce}_{0.6})\text{VO}_4$. The situation for bands at $200\text{--}500\text{ cm}^{-1}$ is quite complicated. The bands at 312 and 357 cm^{-1} are clearly separated even at $x = 0.20$, which implies that the tetragonal scheelite was not formed in this system.

To further study the intrinsic microwave dielectric properties, the infrared reflectivity spectra of $(\text{Bi}_{1-x}\text{Ce}_x)\text{VO}_4$ ceramics were analyzed using a classical harmonic oscillator model:

$$\varepsilon^*(\omega) = \varepsilon_\infty + \sum_{j=1}^n \frac{\omega_{pj}^2}{\omega_{oj}^2 - \omega^2 - j\gamma_j\omega} \quad (5)$$

where $\varepsilon^*(\omega)$ is the complex dielectric function, ε_∞ is the dielectric constant caused by the electronic polarization at high frequencies, γ_j , ω_{oj} and ω_{pj} are the damping factor, the transverse frequency, and plasma frequency of the j th Lorentz oscillator, respectively, and n is the number of transverse phonon modes. The complex reflectivity $R(\omega)$ can be written as

$$R(\omega) = \left| \frac{1 - \sqrt{\varepsilon^*(\omega)}}{1 + \sqrt{\varepsilon^*(\omega)}} \right|^2 \quad (6)$$

The fitted infrared reflectivity values are shown in Figure 9, and the complex permittivities are shown in Figure 10. It is seen

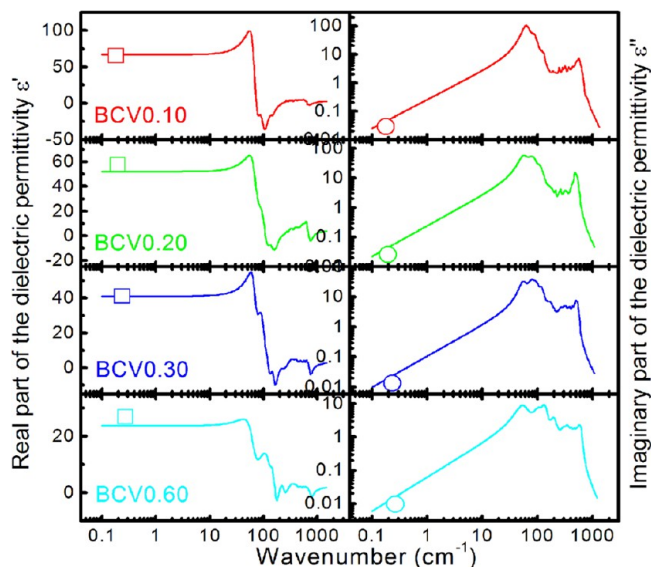


Figure 10. Calculated and measured complex permittivities of the $(\text{Bi}_{1-x}\text{Ce}_x)\text{VO}_4$ ($x = 0.10, 0.20, 0.30, 0.60$) ceramics.

that all the calculated dielectric permittivity and dielectric loss values are almost equal to the measured values using the $\text{TE}_{01\delta}$ method, which implies that majority of the dielectric contribution for this system in the microwave region could be attributed to the absorptions of structural phonon oscillations in the infrared region and there is very little contribution from defect phonon scattering.

CONCLUSIONS

The $(\text{Bi}_{1-x}\text{Ce}_x)\text{VO}_4$ ($x = 0.10, 0.20, 0.30, 0.60$) ceramics can be readily densified below 900 °C . The monoclinic scheelite solid solution of $(\text{Bi}_{1-x}\text{Ce}_x)\text{VO}_4$ can only be formed within $x \leq 0.1$.

In the range composition $0.1 < x \leq 0.6$, a composite phase region with scheelite and zircon phases was formed. The phase equilibrium was influenced by the temperature, and the high temperature can effectively enhance the zircon content in $(\text{Bi}_{1-x}\text{Ce}_x)\text{VO}_4$ ceramics within $0.1 < x \leq 0.6$. When x reaches 0.6, there is almost no scheelite phase observed in the sintered ceramics. The refined values of lattice parameters are $a = 5.1801(0)$ Å, $b = 5.0992(1)$ Å, $c = 11.6997(8)$ Å, and $\gamma = 90.346(0)^\circ$ for the $(\text{Bi}_{0.9}\text{Ce}_{0.1})\text{VO}_4$ sample with the space group $I1_12/b(15)$. The VO_4 tetrahedron contracts with the substitution of Ce for Bi at the A site, and this helps to keep the specific tetrahedron chain stable in the monoclinic structure. Both Raman and infrared analyses supported this result. The best microwave dielectric properties were obtained in the $(\text{Bi}_{0.75}\text{Ce}_{0.25})\text{VO}_4$ ceramic with a permittivity of ~ 47.9 , a Q_f value of ~ 18000 GHz, and a near-zero temperature coefficient of $\sim +15$ ppm/ $^\circ\text{C}$ at a resonant frequency of around 7.6 GHz at room temperature, and the ceramic remains stable in a wide temperature range between 20 and 140 $^\circ\text{C}$. This report offers a novel example to obtain temperature-stable microwave dielectric ceramics by designing a composite sample with two solid solutions with compensating temperature coefficients. This system has the potential to be a good candidate for microwave dielectric resonator and low-temperature cofired technology applications.

AUTHOR INFORMATION

Corresponding Author

*D.Z.: tel (fax), +86-29-82668679; e-mail, zhoudi1220@gmail.com.

Notes

The authors declare no competing financial interest.

ACKNOWLEDGMENTS

This work was supported by the National Science Foundation of China (51202182, 51202178), the International Cooperation Project of Shaanxi Province (2013KW12-04) and the Fundamental Research Funds for the Central University. The authors thank the administrators of the IR beamline workstation of the National Synchrotron Radiation Laboratory (NSRL) for their help in the IR measurements. The SEM work was partially done at International Center for Dielectric Research (ICDR), Xi'an Jiaotong University, Xi'an, People's Republic of China, and the authors thank Ms. Yan-Zhu Dai for her help in using SEM. We also wish to thank the National Science Foundation I/UCRC program, as part of the Center for Dielectric Studies under Grant No. 0628817, for partial support and also the MCL facilities at Penn State University.

REFERENCES

- (1) Sebastian, M. T.; Jantunen, H. *Int. Mater. Rev.* **2008**, *53*, 57–90.
- (2) Axelsson, A. K.; Alford, N. M. *J. Eur. Ceram. Soc.* **2006**, *26*, 1933–1936.
- (3) Zhou, D.; Wang, H.; Pang, L. X.; Randall, C. A.; Yao, X. *J. Am. Ceram. Soc.* **2009**, *92*, 2242–2246.
- (4) Pang, L. X.; Wang, H.; Zhou, D.; Yao, X. *J. Mater. Sci. Mater. Electron.* **2010**, *21*, 1285–1292.
- (5) Suvorov, D.; Valant, M.; Skapin, S.; Kolar, D. *J. Mater. Sci.* **1998**, *33*, 85–89.
- (6) Kim, D. W.; Hong, K. S.; Yoon, C. S.; Kim, C. K. *J. Eur. Ceram. Soc.* **2003**, *23*, 2597–2601.
- (7) Zhou, D.; Randall, C. A.; Wang, H.; Pang, L. X.; Yao, X. *J. Am. Ceram. Soc.* **2009**, *92*, 2931–2936.
- (8) Zhou, D.; Wang, H.; Wang, Q. P.; Wu, X. G.; Guo, J.; Zhang, G. Q.; Shui, L.; Yao, X. *Funct. Mater. Lett.* **2010**, *3*, 253–257.
- (9) Zhou, D.; Wang, H.; Yao, X.; Pang, L. X. *J. Am. Ceram. Soc.* **2008**, *91*, 2228–2231.
- (10) Zhou, D.; Wang, H.; Yao, X.; Pang, L. X.; Chen, Y. H. *Mater. Chem. Phys.* **2009**, *113*, 265–268.
- (11) Li, L.; Chen, X. M. *Mater. Lett.* **2009**, *63*, 252–254.
- (12) Li, L.; Chen, X. M.; Fan, X. C. *J. Eur. Ceram. Soc.* **2006**, *26*, 2817–2821.
- (13) Li, L.; Chen, X. M. *J. Am. Ceram. Soc.* **2006**, *89*, 2514–2520.
- (14) Zhou, D.; Pang, L. X.; Guo, J.; Qi, Z. M.; Shao, T.; Yao, X.; Randall, C. A. *J. Mater. Chem.* **2012**, *22*, 21412–21419.
- (15) Panchal, V.; Lopez-Moreno, S.; Santamaria-Perez, D.; Errandonea, D.; Manjon, F. J.; Rodriguez-Hernandez, P.; Munoz, A.; Achary, S. N.; Tyagi, A. K. *Phys. Rev. B* **2011**, *84*, 024111.
- (16) Hirata, T.; Watanabe, T. *J. Solid State Chem.* **2001**, *158*, 264–267.
- (17) Zhou, D.; Qu, W. G.; Randall, C. A.; Pang, L. X.; Wang, H.; Wu, X. G.; Guo, J.; Zhang, G. Q.; Shui, L.; Wang, Q. P.; Liu, H. C.; Yao, X. *Acta Mater.* **2011**, *59*, 1502–1509.
- (18) Zhou, D.; Pang, L. X.; Wang, H.; Guo, J.; Yao, X.; Randall, C. A. *J. Mater. Chem.* **2011**, *21*, 18412–18420.
- (19) Zhou, D.; Pang, L. X.; Guo, J.; Wang, H.; Yao, X.; Randall, C. A. *Inorg. Chem.* **2011**, *50*, 12733–12738.
- (20) Sleight, A. W.; Chen, H. Y.; Ferretti, A.; Cox, D. E. *Mater. Res. Bull.* **1979**, *14*, 1571–1581.
- (21) Dreyer, G.; Tillmanns, E. *Neues Jahrb. Mineral., Monatsh.* **1981**, *4*, 151–154.
- (22) Hirata, T.; Watanabe, A. *J. Solid State Chem.* **2001**, *158*, 264–267.
- (23) Rao, R.; Garg, A. B.; Wani, B. N. *J. Phys.: Conf. Ser.* **2012**, *377*, 012010.
- (24) Hirata, T.; Watanabe, A. *J. Solid State Chem.* **2001**, *158*, 254–259.
- (25) Opara-Krasovec, U.; Orel, B.; Surca, A.; Bukovec, N.; Reisfeld, R. *Solid State Ionics* **1999**, *118*, 195–214.
- (26) Baran, E. J.; Aymonino, P. *J. Z. Anorg. Allg. Chem.* **1971**, *383*, 226–229.
- (27) Baran, E. J.; Escobar, M. E.; Fournier, L. L.; Filgueira, R. R. *Z. Anorg. Allg. Chem.* **1981**, *472*, 193–199.
- (28) Hardcastle, F. D.; Wachs, I. E. *J. Phys. Chem.* **1991**, *95*, 5031–5041.
- (29) Santha, N.; Sebastian, M. T.; Mohanan, P.; Alford, N. M.; Sarma, K.; Pullar, R. C. *J. Am. Ceram. Soc.* **2004**, *87*, 1233–1237.
- (30) Heydweiller, A. *Z. Phys.* **1920**, *3*, 308–317.
- (31) Shannon, R. D. *J. Appl. Phys.* **1993**, *73*, 348–366.
- (32) Feteira, A.; Sinclair, D. C.; Lanagan, M. T. *J. Appl. Phys.* **2007**, *101*, 064110.
- (33) Jacob, M. V.; Mazierska, J.; Krupka, J. *J. Electroceram.* **2005**, *15*, 237–241.
- (34) Gotic, M.; Music, S. *J. Mol. Struct.* **2005**, *535*, 744–777.
- (35) Tolstoy, V. P.; Tolstobrov, E. V. *Solid State Ionics* **2002**, *151*, 165–169.
- (36) Liu, J. B.; Wang, H.; Wang, S.; Yan, H. *Mater. Sci. Eng.* **2003**, *B104*, 36–39.